Copyright © 1967, by the author(s).
All rights reserved.

Permission to make digital or hard copies of all or part of this work for personal or classroom use is granted without fee provided that copies are not made or distributed for profit or commercial advantage and that copies bear this notice and the full citation on the first page. To copy otherwise, to republish, to post on servers or to redistribute to lists, requires prior specific permission.

SCANNING ELECTRON MICROSCOPE INVESTIGATION OF PLANAR DIFFUSED P-N JUNCTION PROFILES NEAR THE EDGE OF A DIFFUSION MASK

by

N. C. MacDonald and T. E. Everhart

Memorandum No. ERL-M199

27 January 1967

ELECTRONICS RESEARCH LABORATORY

College of Engineering
University of California, Berkeley
94720

Manuscript submitted: 21 December 1966

The research reported herein was supported by the Research and Technology Division, Air Force Avionics Laboratory, Wright-Patterson Air Force Base, Ohio, under Contract No. AF 33(615)-3886. The work was performed on the Berkeley Scanning Electron Microscope-I, which was constructed with the support of the Research and Technology Division, Air Force Avionics Laboratory, Wright-Patterson Air Force Base, Ohio, under Contract AF 33(615)-1045 and 2306; the Joint Services Electronics Program (U. S. Army, U. S. Navy, and U. S. Air Force) under Grant No. AF-AFOSR-139-64; and the University of California, Berkeley.

One of the authors of this report, N. C. MacDonald, is a National Science Foundation Trainee.

ACKNOWLEDGMENT

The authors wish to acknowledge the assistance of Mrs. D. McDaniel for mounting and bonding the devices used for this research. The donation of transistors by ITT Laboratories is greatly appreciated.

One of us (N. C. MacD.) wishes to acknowledge the financial support received from the National Science Foundation Traineeship program.

ABSTRACT

A scanning electron microscope is used to determine the geometry of a planar p-n junction profile near the edge of a diffusion mask. The planar junctions are angle-lapped at large angles (~ 45°) to expose the cross section of the p-n junction. Computer calculations of the theoretical p-n junction profiles are presented. The theoretical profiles, normalized with respect to the junction depth, are presented as a function of the lap angle, the angle the lapped surface makes with the electron probe, and the ratio of the bulk impurity concentration to the impurity concentration at the surface. The normalized theoretical profiles are found to compare quite well with the experimental profiles obtained with the Berkeley Scanning Electron Microscope-I.

TABLE OF CONTENTS

	Page No.
INTRODUCTION	1
THEORY	2
EXPERIMENTAL PROCEDURE AND THEORETICAL CALCULATIONS	5
EXPERIMENTAL RESULTS AND DISCUSSION	9
FURTHER DISCUSSION	13
REFERENCES	16
TABLES	18
LIST OF FIGURES	20

I. INTRODUCTION

Planar silicon devices and integrated circuits are fabricated by selectively introducing impurities into silicon. Impurities can be selectively diffused into the silicon substrate by opening windows in a diffusion masking material. For an opening a few times greater than the diffusion depth, the diffusion process is essentially one-dimensional away from the edges of the opening. Near the edges of the opening of the diffusion mask, lateral diffusion occurs beneath the diffusion mask. An analysis of the impurity atom distribution near the diffusion mask for a planar p-n junction was performed recently by Kennedy and O'Brien.[1] They present a mathematical discussion of the concentration profile and the concentration gradient of a diffused junction. The two-dimensional p-n junction profiles for an instantaneous source diffusion (ISD) and a constant surface concentration diffusion (CSCD) are presented in Ref. 1; the junction profiles (or constant concentration profiles) are normalized with respect to $(\pi Dt)^{1/2}$.

In this paper we compare the theoretical two-dimensional junction profiles with experimentally obtained profiles. The Berkeley Scanning Electron Microscope-I[2] is used to probe angle-lapped, planar p-n junctions. The high magnification of the scanning electron microscope (SEM) together with its capability to detect the high field region of p-n junctions[3,4] provides a powerful tool for studying two-dimensional diffusion phenomena.

First, a simple derivation of the two-dimensional ISD diffusion profile at the edge of an oxide mask is given. The junction profiles are then plotted for both the ISD and CSCD. The junction profiles are normalized with respect to the junction depth to facilitate comparison of the theoretical and experimental junction profiles. Next, micrographs of angle-lapped p-n junction profiles are compared with the theoretical predictions. Theoretical profiles for practical light microscope observation and for SEM observation are compared and discussed.

II. THEORY

In this section a sketch of the derivation for an instantaneous source diffusion ISD is presented to introduce the nomenclature used in the remainder of the text. The theoretical results of the two-dimensional solution to the diffusion equation for a constant surface concentration diffusion are also presented.

Figure 1a illustrates a rectangular opening in the oxide for a subsequent diffusion. Ideally, the oxide acts as a diffusion mask, and impurities are selectively introduced into the silicon in the rectangular region where the oxide is removed. A partial section through the rectangular opening in the oxide is shown in Fig. 1b. The origin of coordinates is taken as the edge of the oxide mask. An n-type substrate of impurity concentration C_B is assumed. If a line source of p-type impurities of strength Q and positioned

at coordinates (0, y') is diffused into the semiconductor a p-n junction is formed when the concentration of the p-type impurities C_ℓ is equal to C_B. The impurities diffuse into the semiconductor in accordance with the two-dimensional isotropic diffusion equation, Eq. (1) where D is the diffusion constant of the impurity. A solution of Eq. (1) for a line source of

$$\frac{\partial C}{\partial t} = D \nabla_{xy}^2 C \tag{1}$$

a constant number of impurity atoms is given by Eq. (2).[5]

$$C_\ell = Q \exp \frac{x^2 + (y - y')^2}{4Dt} \tag{2}$$

The shape of the p-n junction profile for a line source is shown by the dotted line in Fig. 1b.

If y' in Eq. (2) approaches zero, a portion of the p-n junction lies to the right of the oxide edge. For diffusion at the oxide edge illustrated in Fig. 1b, the effect of lateral diffusion to the right of the oxide edge is considered to arise from line sources distributed from $0 < y' < -\infty$.[5] The two-dimensional p-n junction profile is obtained by integrating the solution Eq. (2) over y'. The result is given by the following expression

$$C(x, y, t) = \frac{Q}{\sqrt{2\pi Dt}} \exp\left(\frac{-x^2}{4Dt}\right) \operatorname{erfc}\left(\frac{y}{\sqrt{4Dt}}\right) . \tag{3}$$

After diffusion for a time $t = \tau$, the p-n junction profile forms at the coordinates (x, y) where $C(x, y, \tau) = C_B$. By applying Eq. (3), the shape of the profile is given by the expression

$$C_R \equiv \frac{C_B}{C_0} = \frac{1}{2} \exp\left(\frac{-x^2}{4Dt}\right) \operatorname{erfc}\left(\frac{y}{\sqrt{4D\tau}}\right) , \qquad (4)$$

where $C_0 = Q/\sqrt{\pi D \tau}$. For $y << 0$ the diffusion is one-dimensional, and Eq. (4) reduces to the familiar one-dimensional Gaussian impurity distribution. In the one-dimensional region, the junction forms at a depth x_j from the surface of the semiconductor. A sketch of the p-n junction profile is given by the dashed curve in Fig. 1c. In Sec. III, Eq. (4) is used to calculate the p-n junction profiles for various values of C_R in order to study the lateral diffusion that occurs at the edge of a diffusion mask. Extension of the analysis for an ISD for anisotropic diffusion i.e., $D_x \neq D_y$ is also tractable.

Diffusion can also be performed from a source that maintains a constant concentration C_0 of impurities at the surface of the semiconductor. The two-dimensional solution of Eq. (1) for a constant C_0 for $-\infty < y < 0$ is given by Eq. (5).[1]

$$C(r, \theta, t) = C_0 \left\{ 1 - 2\pi \sum_{n=0}^{\infty} \sin\left[\left(n + \frac{1}{2}\right)\theta'\right] \frac{\left[r/2\sqrt{Dt}\right]^{n+1/2} \Gamma\left[(n + 1/2)/2\right]}{2\Gamma(n + 3/2)} \cdot M\left[\frac{n + 1/2}{2} ; (n + 3/2) ; -r^2/4Dt\right] \right\} \qquad (5)$$

where

$$\theta' = \theta + \pi \qquad 0 < \theta < \pi ,$$

and

$$M(a, b, z) = \sum_{k=0}^{\infty} \frac{a_k z^k}{k! \beta_k}$$

$$a_k = a(a+1)(a+2) \cdot \cdot \cdot (a+k-1), \quad a_0 = 1$$

$$b_k = b(b+1)(b+2) \cdot \cdot \cdot (b+k-1), \quad b_0 = 1$$

The coordinates (r, θ) are shown in Fig. 1c. Note that for each value of C the series M must be evaluated for each coefficient of the series for C. The p-n junction profile after diffusion for a time τ is obtain by setting $C(r, \theta, \tau) = C_B$ and solving Eq. (5) for r and θ.

III. EXPERIMENTAL PROCEDURE AND THEORETICAL CALCULATIONS

Observation of the junction profile is performed by using the scanning electron microscope (SEM)[2-4] to probe angle-lapped planar p-n junctions. Figure 2a is an illustration of an oxide masked p-n junction specimen that is angle-lapped[6] to expose the junction profile. The lap-angle is β, and the point (0) is the edge of the oxide mask. Figure 2b shows the position of the device relative to the electron beam. The specimen mount subtends an angle α with the incident beam. To obtain a micrograph of the diffusion profile, an electron beam of approximately 0.1 μm in diameter is scanned over the lapped surface of the device; the resulting secondary electrons are collected to provide a video signal which modulates the intensity of a

synchronously scanned cathode-ray tube (CRT). A photograph of the CRT is the SEM micrograph. The potential step across the p-n junction produces the contrast. It is also possible to modulate the CRT by a signal that is proportional to the electron beam-induced current (EBIC) in the p-n junction.

With reference to Fig. 2b, the micrograph displays the projection of the junction profile on a plane perpendicular to the electron beam. The slope of the projected profile is a function of the angles α and β. By simple geometrical considerations, the actual x coordinate of the junction profile is related to the length x_m observed on the micrograph by the following expression

$$x_m = x \left[\frac{\sin(\alpha + \beta)}{\sin(\beta)} \right] . \quad (6)$$

For a comparison of the theoretical and the experimental results it is necessary to calculate the diffusion profiles with the angles α and β as parameters. It is expedient to normalize the coordinates with respect to the junction depth x_j in the one-dimensional diffusion region, because the normalized value of x_j is easily related to the junction depth that is observed on the micrograph.

Computer solutions of Eqs. (3) and (5) were obtained for various values of C_R and for various angles α and β. The pertinent results of the computer calculations are shown in Figs. 3 through 5. Figure 3a and b show the theoretical shape of the junction profiles for an ISD and a CSCD, respectively.

The profiles are calculated for $C_R = 10^{-2}$, 10^{-3} and 10^{-5}, and the coordinates are normalized by the value for x_j for each value of C_R. With reference to Figs. 3a and b, the lateral diffusion under the oxide mask approaches the magnitude of x_j as C_R decreases. Note also that, in order to match the theoretical curves to experimental curves, C_R must be known only to an accuracy of the order of fifty percent; the shape of the normalized junction profiles are not a strong function of C_R. A comparison between the normalized junction profiles for an ISD (solid line) and CSCD (points) with $C_R = 10^{-2}$ is shown in Fig. 3c. Referring to Fig. 3c, we can see that once the profiles are normalized to their respective x_j's the shapes of the profiles for the same C_R are nearly identical. This latter fact facilitates the process of comparing the theoretical and experimental results because the actual comparison of the normalized junction profiles will not depend strongly on the exact initial condition, i.e., ISD or CSCD. The fact that the normalized profiles for an ISD and CSCD are nearly the same also facilitates the calculation of the two-dimensional profiles. The closed-form solution for the ISD, Eq. (5), is much easier to use in comparison with the solution for the CSCD, Eq. (5).

The projected shapes of the junction profiles as a function of α and β for $C_R = 10^{-5}$ are shown in Figs. 4 and 5. The profiles are normalized with respect to x_j for $C_R = 10^{-5}$, and the shape of the curve is the projection of the profile on a plane perpendicular to the electron beam (see Fig. 2). The

junction profiles for $\alpha = 45°$ and β as a parameter are illustrated in Fig. 4. As the lap angle is reduced, the projected junction depth x_{jm} increases, but the lateral coordinate y remains the same. Hence, the value of x_{jm} can be measured with a greater degree of accuracy with a corresponding loss of accuracy in measuring the y coordinate. Junction profiles for $\beta = 60°$ and α as a parameter are shown in Fig. 5. The elongation of the x coordinate is seen to be small over the range $15° < \alpha < 30°$, and hence, for this range of values for α the projected profile is less sensitive to changes in the magnitude of the angle α. Furthermore, Fig. 5 illustrates the fact that if $\alpha = \beta = 60°$ the projected profile is identical to the actual junction profile; this is expected since substitution of $\alpha = \beta = 60°$ in Eq. (6) yields $x_m = x$.

The pertinent results of the theoretical calculations are summarized as follows: once the profiles are normalized with respect to x_j for a given value of C_R, the shape of the normalized diffusion profile does not depend strongly on C_R, and consequently, C_R does not have to be known to a high degree of accuracy in order to compare the theoretical calculations with the experimental profiles. If the junction profiles for a given C_R for an ISD and a CSCD are normalized with respect to their respective x_j's, the normalized junction profiles are nearly identical. By a proper choice of α and β the sensitivity of the shape of the junction profile to small changes or inaccuracies in either α or β can be minimized. A choice of $\alpha = \beta = 60°$ projects the actual junction profile on a plane perpendicular to the electron beam.

IV. EXPERIMENTAL RESULTS AND DISCUSSION

A micrograph of the channel region of a junction field-effect transistor is shown in Fig. 6. The device is mounted relative to the electron beam as shown in Fig. lb with $\alpha = 45°$ and the lap angle $\beta = 60°$. Figure 6a illustrates the geometry of the device as it appears on the micrograph. The regions shown are the n oxide-masked diffused gate, the n^+ substrate gate, and the p-type epitaxial layer. The dimensions x_{jm} and x_{em} represent the projected depth of the diffused junction and the projected thickness of the p-type epitaxial layer, respectively. Estimates of the magnitude of the junction depth x_j and the thickness of the epitaxial layer x_e are obtained by three methods: groove and stain, bevel and stain, and the scanning electron microscope. Table I lists the magnitude of x_j and x_e for the three techniques; this latter fact lends support to the claim that the black-gray contrast observed on the micrographs of Fig. 6 is essentially the p-n junction profile.[3,4] A reverse bias of approximately 3 volts is applied to the p-n junctions shown in Fig. 3. This corresponds to a depletion layer width of approximately 0.8 μm, and the width of the depletion region produces further error in any absolute measurement of x_j from the micrographs of Fig. 6. Further discussion of the accuracy of the SEM measurements is presented below.

For a comparison between the shape of the experimental diffused p-n junction profile and the theoretical p-n junction profile, only a relative

measurement of the coordinates is required. The pertinent properties of the p-n junction devices discussed in this paper are listed in Table 2. We are now concerned with the column labeled Fig. 6 of Table 2. A solution of Eq. (4) with $C_R = 10^{-5}$ and normalized with respect to the value of x_{jm} is shown superimposed on the micrograph in Fig. 6b. With reference to Fig. 6b, the experimental and the theoretical profiles are seen to compare quite well. The point labeled 0 is the origin of the coordinates and the edge of the oxide window for the diffusion. A slight black-gray contrast is observed on the micrograph where the oxide step occurs.

A micrograph of four emitter stripes of a comb-structure commercial bipolar transistor is shown in Fig. 7a. The arrow points to the edge of the lapped surface. The known properties of the device shown in Fig. 7 are listed under the appropriate column in Table 2. The comb structure allows one to evaluate the uniformity of the lapping technique as well as the uniformity of the emitter diffusions. It is evident from Fig. 7a that the angle lap is quite uniform for all four emitter stripes. A higher magnification micrograph of one of the emitter stripes is shown in Fig. 7b. By increasing the magnification in a stepwise fashion, the approximate position of the edge of the diffusion mask is more easily obtained. With reference to Fig. 7b, the lapped surface is marked by the letter A, the aluminum electrode on the surface of the emitter stripe is marked by the letter B, and the point that marks the approximate edge of the diffusion mask is labeled with the letter O.

Figure 8 shows a high magnification micrograph of one side of a planar-diffused emitter stripe shown in Fig. 7. The value for C_R is estimated from practical values of C_B and C_0 for commercial bipolar transistor structures. Points calculated using Eq. 4 with a value for $C_R = 10^{-5}$ are superimposed on the micrograph of Fig. 8a. Again, the theoretical and experimental p-n junction profiles agree quite well. An estimate of the error involved in choosing different values for C_R is obtained by plotting the p-n juntion profiles for $C_R = 10^{-3}$ and $C_R = 10^{-6}$; the theoretical profiles normalized with respect to x_{jm} are presented in Fig. 8b. The close proximity of the two profiles of Fig. 8b justifies the seemingly deceptive choice of $C_R = 10^{-5}$ for the theoretical profile shown in Fig. 8a.

In practice, the actual kinetics for diffusion of impurities into the semiconductor is not strictly represented by the isotropic, field independent diffusion equation, Eq. (1).[7] Also, the boundary conditions do not correspond strictly to an ISD or CSCD in practical semiconductor device manufacturing steps. For shallow emitter diffusions, the objections to the use of Eq. (1) and the corresponding solutions, Eqs. (3) and (5), to describe the p-n junction profile are quite valid, but even the emitter diffusion junction profile shown in Fig. 8 is approximated quite well by Eq. (4). That is to say, once the theoretical results are normalized with respect to the actual junction depth x_j (or x_{jm}), Eq. (4) appears to be a good approximation to the shape of the p-n junction profile.

The contrast for the micrographs of Figs. 6 through 8 is obtained by measuring the relative number of secondaries that are collected from a given area of the specimen. Contrast can also be obtained by using the electron-beam-induced current EBIC from different positions on the specimen to modulate the CRT or deflection modulation display. A combination of both secondary electron contrast and EBIC contrast is helpful for the investigation of various diffusion phenomena. A poor quality p-n junction is shown in Fig. 9. The properties of the junction are listed in the appropriate column of Table 2. The thickness of the oxide mask for the diffusion of phosphorous is approximately 0.2 μm, and consequently, some diffusion of the impurity through the oxide occurred.[8] Figure 9a shows a low magnification secondary emission micrograph of the p-n junction, the arrows 1 and 2 locate a diffusion defect in the planar-diffused p-n junction and the p-n junction formed by diffusion of the impurities through the oxide, respectively. A highly magnified secondary emission micrograph of the poor quality junction is shown in Fig. 9b. The defect located by arrow 1 is probably the result of enhanced diffusion in this region due to an initial defect in the starting wafer. Arrow 2 points to a ragged dark region at the edge of the angle-lapped surface. It could be argued that the dark region located by arrow 2 in Fig. 9b is the result of a poor quality angle lap that has damaged the surface near the edge of the angle lap such that the surface appears at the same potential as the p-n junction. The EBIC micrograph in Fig. 9c shows a large signal

(white areas) both around the edge of the planar p-n junction and on the oxide-covered surface A. An explanation of the contrast shown on the micrograph of Fig. 9c is obtained with the aid of Fig. 10. With reference to Fig. 10, the boundary of the diffused region is shown to include the diffused junction beneath the oxide. The p-n junction is reverse biased and hence EBIC is observed when electron-hole pairs are created in the depletion region of the junction. The 10 kV primary electrons easily penetrate the thin layer of oxide, and a large EBIC current is observed if a shallow p-n junction or inversion layer lies below the Si - SiO_2 interface. Hence, the large EBIC observed on the oxide-covered surface A of Fig. 9c is due to the fact that diffusion of impurities through the oxide has resulted in a shallow p-n junction beneath the oxide surface. It should be noted that in order to detect the existence of a diffused junction beneath the oxide, an angle-lapped device is not required. The depth of the p-n junction is measured by using an angle-lapped specimen and obtaining a micrograph similar to Fig. 9b. The smallest junction depth that can be measured by this technique is somewhat limited by the transverse scattering of the electron beam.

V. FURTHER DISCUSSION

The junction depth is also measured by viewing a bevel and stained p-n junction device with an optical microscope. Since the magnification of the optical microscope is much less than that of the SEM, the lap angle β must

be very small, typically 5°, in order to elongate the x coordinate of the junction profile; a corresponding reduction in the y coordinate of the profile occurs. Junction profiles calculated using Eqs. (4) and (6) with the light probe or electron beam normal to the lapped surface ($\alpha = 90° - \beta$) are shown in Fig. 11. The junction profiles of Fig. 11 are normalized with respect to x_{jm}. For a light probe, the profile with $\beta = 5°$ is appropriate. Actual measurement of the shape of the profile for $\beta = 5°$ is quite difficult because the profile rises quite rapidly for $y > 0$. The higher magnification of the SEM allows the use of large values for β, and the two-dimensional shape of the junction profile is quite discernible. Profiles with $\beta = 45$ and $90°$ are compared with the profile for $\beta = 5°$ in Fig. 11.

In addition to the advantages of the higher magnification and the greater depth of focus of the SEM over the light microscope, the SEM locates the p-n junction without any intermediate step such as staining. It is not at all obvious that the contrast formed by the stain actually delineates the boundary of the p-n junction. With the scanning electron microscope, the EBIC mode of operation can be used to detect the high field region between the p and n regions of the semiconductor. In fact, the p-n junction can be slightly forward-biased to reduce the width of the depletion region.[3,4] The ability to correlate accurately the maximum EBIC with the actual position of the p-n junction on the lapped surface requires some qualifications. In particular, the position on the lapped surface where the maximum electric field

occurs is a function of both the angle β and the nature of the concentration profile for the p-n junction.[9] The larger the value of β and the more abrupt the p-n junction, the better the accuracy in determining the junction profile. The devices discussed in the previous sections of this paper had high values for C_0 ($\sim 10^{20}$ cm^{-3}) and large values for β ($\beta \geq 45°$), and consequently, the junction profiles should be easily defined within the accuracy of transverse scattering of the electron beam (< 0.3 μm).[10]

Simple, planar p-n junctions have been considered in this paper, but complex structures with multiple diffusions can also be investigated with the SEM.[3,4,11] Various two-dimensional diffusion phenomena can be studied with techniques similar to those discussed above. Present solid-state integrated circuit structures use multiple diffusion processes to obtain isolation between various devices and to obtain the desired device properties. As the packing densities of these structures increase, the three-dimensional nature of the semiconductor substrate will become more important. The SEM should prove to be very useful in research and development of integrated circuits.

REFERENCES

1. D. P. Kennedy and R. R. O'Brien, "Analysis of the impurity atom distribution near the diffusion mask for a planar p-n junction," IBM J. Research Develop., Vol. 9, 179 (May 1965).

2. C. W. Oatley, W. C. Nixon and R. F. W. Pease, "Scanning electron microscopy," Advances in Electronics and Electron Physics, Vol. 21, (Academic Pres, New York, 1964), p. 181.

3. N. C. MacDonald and T. E. Everhart, "Direct measurement of the depletion layer width variation vs applied bias for a p-n junction," Appl. Phys. Letters, Vol. 7, 267-269 (1965).

4. T. E. Everhart et. al., "Applications of the scanning electron microscope to semiconductor devices," Electron Microscopy 1966, Vol. I, (Maruzen Co., Ltd., Tokyo).

5. H. S. Carslaw and J. C. Jaeger, Conduction of Heat in Solids, (Oxford University Press, 1959), Second Edition, Chap. X.

6. The final lap and polish is made with Linde A lapping compound.

7. N. B. Hannay, editor, Semiconductors, (Reinhold Publishing Corporation, New York, 1959), Chap. 6.

8. C. T. Sah, H. Sillo and D. A. Tremere, J. Phys. Chem. Solids, Vol. 11, p. 288, (1959).

9. R. L. Davies and F. E. Gentry, "Control of electric field at the surface of p-n junctions," IEEE Trans. on Electric Devices, Vol. ED-11, No. 7, pp. 313-323 (July 1964).

10. R. F. W. Pease, "The spatial distribution of secondary electron emission," paper presented at the 2nd International Conf. on Electron and Ion Beam Sci. and Tech., New York, (1966).

11. N. C. MacDonald and T. E. Everhart, "Some observations on angle lapped and cleaned p-n junction devices," paper presented at the 2nd International Conf. on Electron and Ion Beam Sci. and Tech., New York, (1966).

TABLE I

Measurements of the junction depth and epitaxial layer thickness of the device in Fig. 6.

TECHNIQUE	x_j (μm)	Epitaxial layer THICKNESS (μm)
GROOVE and stain[a, b]	6.1 ± 0.3	9.5 ± 0.3
BEVEL and stain[a, b, c]	---	9.6 ± 0.4
SCANNING ELECTRON MICROSCOPE[b]	5.9 ± 0.3	9.2 ± 0.3

[a] Stained with HF acid and placed under a spotlight.

[b] Scaled from a micrograph.

[c] 4° 17' bevel.

TABLE II[a]

Device Parameters

Device	FIGURE 6 Junction Field-Effect Transistor[b]	FIGURES 7, 8 Commercial Bipolar Transistor	FIGURE 9 Diffused p-n Junction[b]
C_B	$8. \times 10^{15}$ cm^{-3}	---	10^{16} cm^{-3}
C_R	$2. \times 10^{-5}$	$\sim 10^{-5}$ [d]	3×10^{-5}
x_j	6 μm[c]	~ 1.8 μm	3 μm
α	45°	45°	45°
β	60°	45°	45°
reverse bias (volts)	3	3	2.8

[a]Accelerating voltage is 10 kV.

[b]Device fabricated in the Semiconductor Laboratory at the University of California, Berkeley.

[c]See Table I.

[d]Estimate. See text for further comment.

LIST OF FIGURES

Fig. 1. Illustration of the selected diffusion of impurities into a semiconductor.

Fig. 2. Schematic diagram illustrating: (a) the geometry of the angle lapped specimen and (b) the position of the angle-lapped specimen relative to the electron beam probe.

Fig. 3. Theoretical diffusion profiles normalized with respect to the junction depth x_j. (a) Instantaneous source diffusion, (b) Constant surface concentration diffusion and (c) Comparison of the $C_R = 10^{-2}$ junction profiles of (a) and (b).

Fig. 4. Theoretical junction profiles for $\alpha = 45°$ and $\beta = 15°$, 30°, 45° and 60° and 90° (actual junction profile).

Fig. 5. Theoretical junction profiles for $\beta = 60°$ and $\alpha = 15°$, 30 °, 45°, 60° and 90° (actual junction profile).

Fig. 6. Micrograph of an angle-lapped ($\beta = 60°$) planar-diffused p-n junction. (a) A micrograph illustrating the projected junction depth x_{jm} and the projected thickness x_{em} of the p-type silicon epitaxial layer. (b) Same micrograph as in (a) with the theoretical curve calculated from Eqs. 4 and 8 superimposed on the profile observed with the scanning electron microscope.

Fig. 7. Micrographs of a comb-structure bipolar transistor that is angle-lapped with $\beta = 45°$. (a) Four emitter stripes of the bipolar transistor are shown. (b) Higher magnification micrograph of a single, reverse-biased emitter stripe.

Fig. 8. Experimental and theoretical junction profiles for the emitter diffusions shown in Fig. 7. (a) A high magnification micrograph of a diffused emitter stripe with the theoretical profile for $C_R = 10^{-5}$ superimposed on the experimental profile. (b) Theoretical profiles illustrating the variation of the normalized p-n junction profile for $C_R = 10^{-3}$ and 10^{-6}.

Fig. 9. Micrographs of a poor quality p-n junction. (a) Low magnification secondary emission micrograph of the angle-lapped diffused junction. (b) A higher magnification secondary emission micrograph of the junction shown in (a). (c) Electron beam induced current micrograph of the region shown in (b).

Fig. 10. Schematic diagram showing the diffused junction and depletion region beneath the oxide.

Fig. 11. Theoretical p-n junction profiles for $C_R = 10^{-3}$ and $\beta = 5°$, $45°$, and $90°$. The curve for $\beta = 5°$ corresponds to the usual shape of the profile when it is observed with a light microscope.

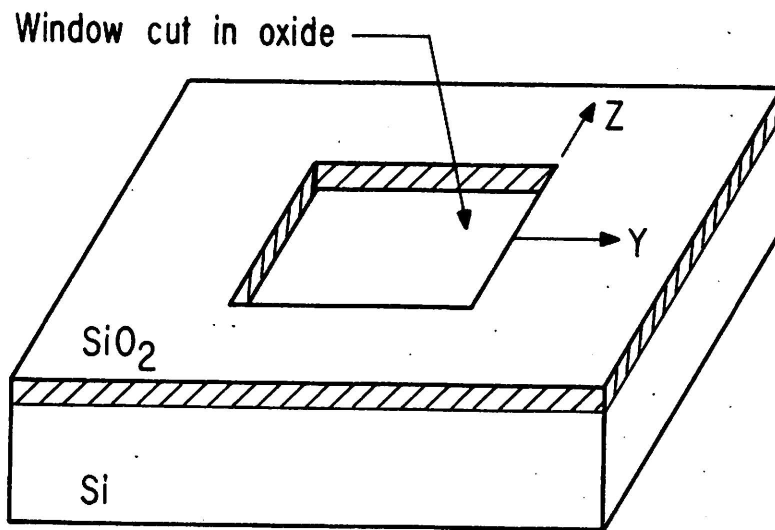

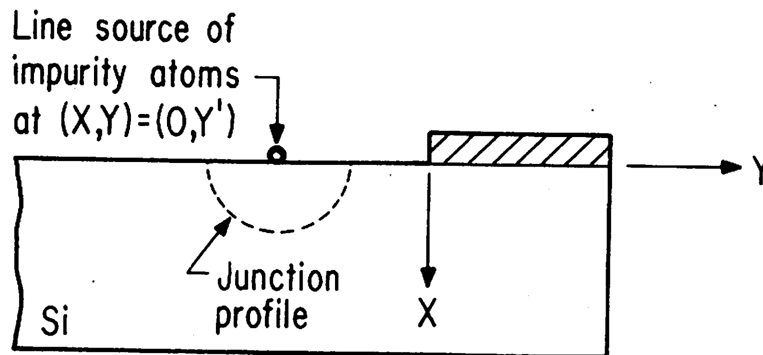

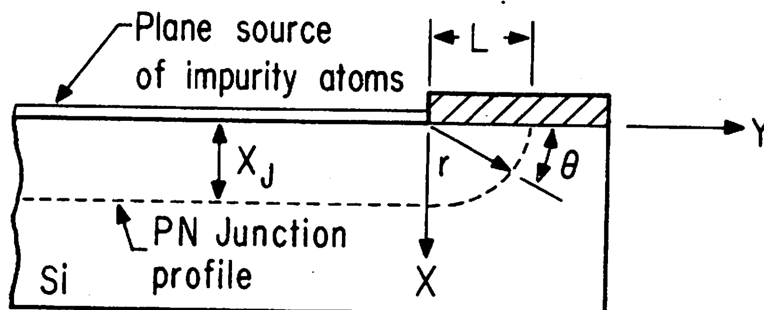

Fig. 1.

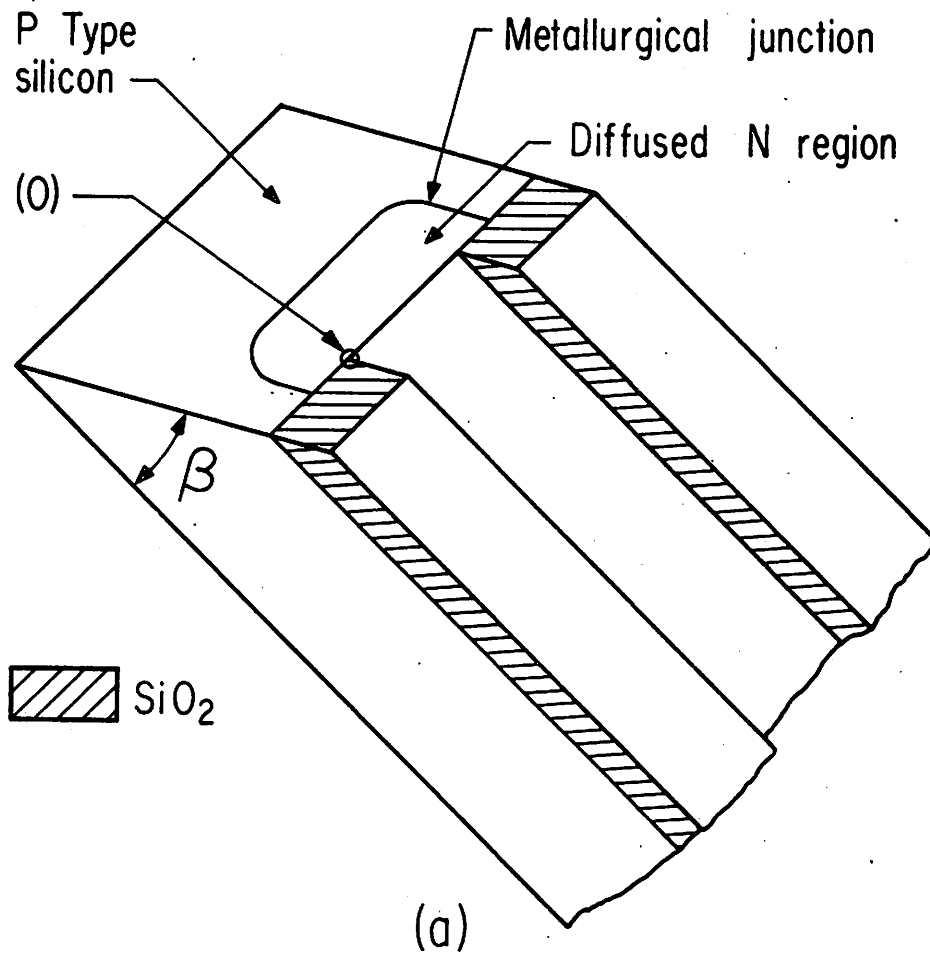

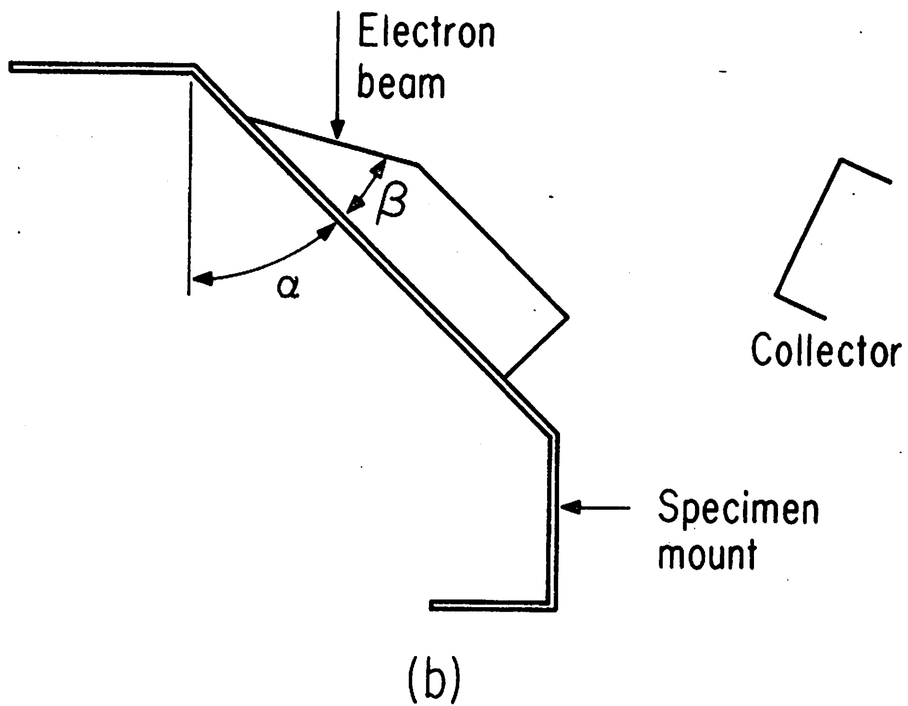

Fig. 2.

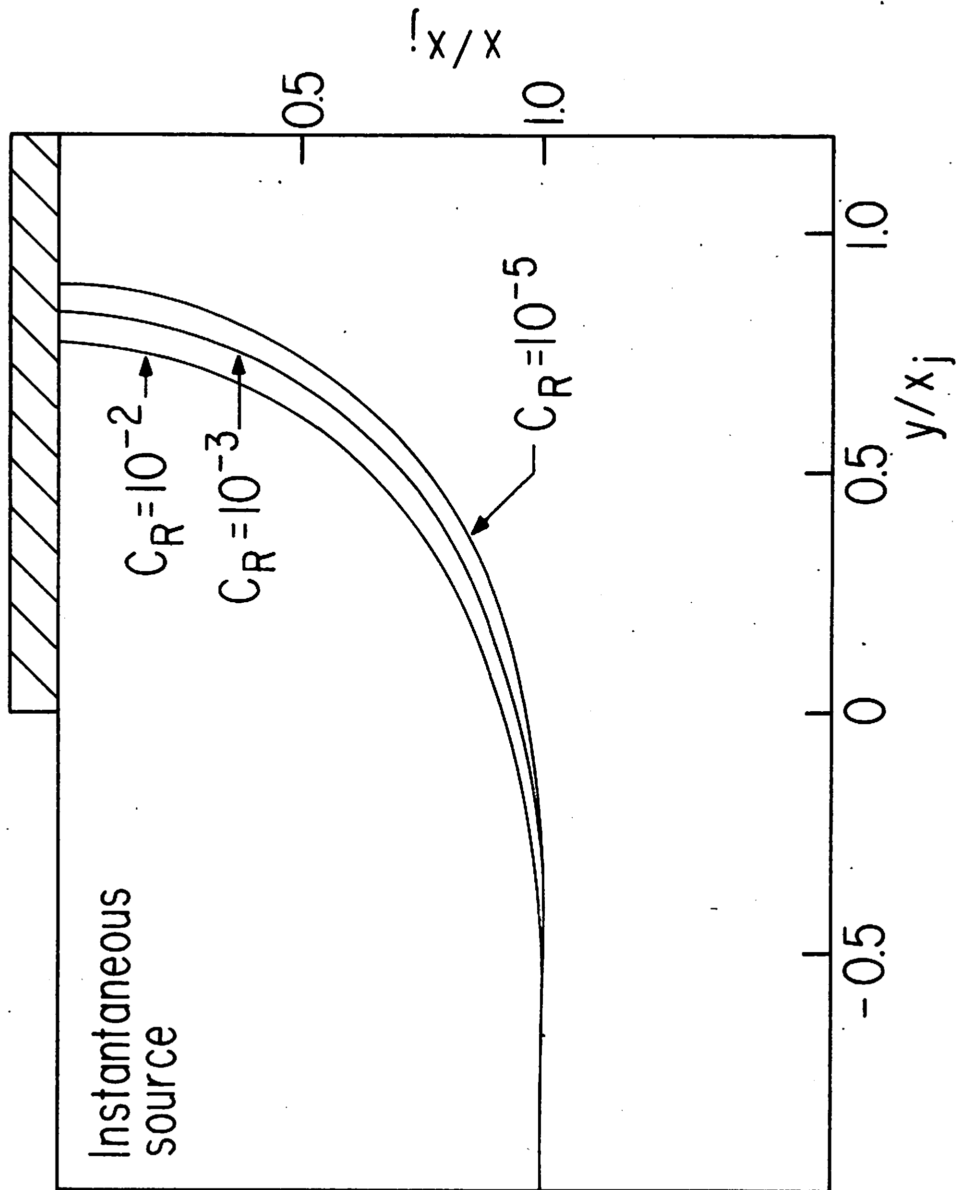

Fig. 3 a.

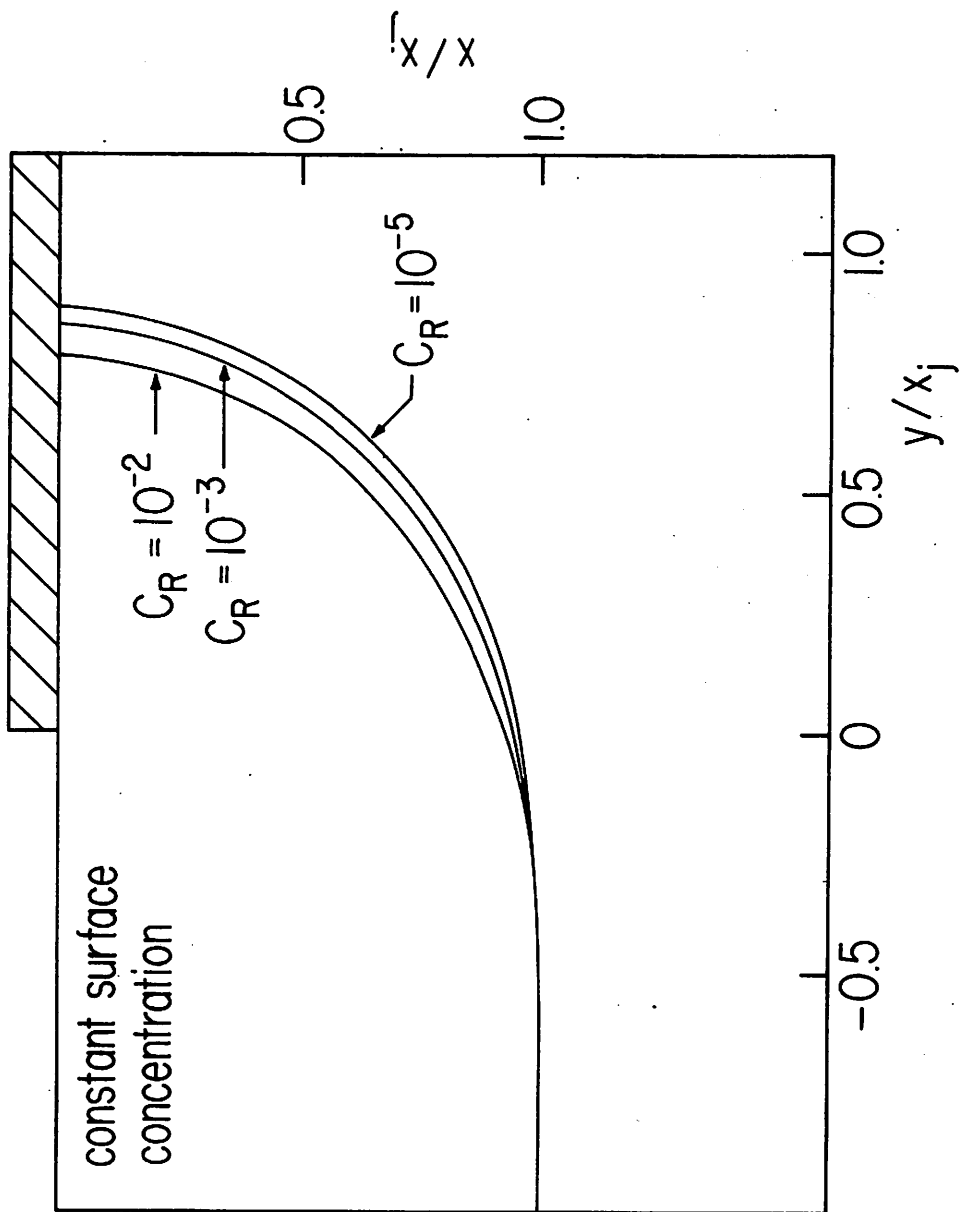

Fig. 3 b.

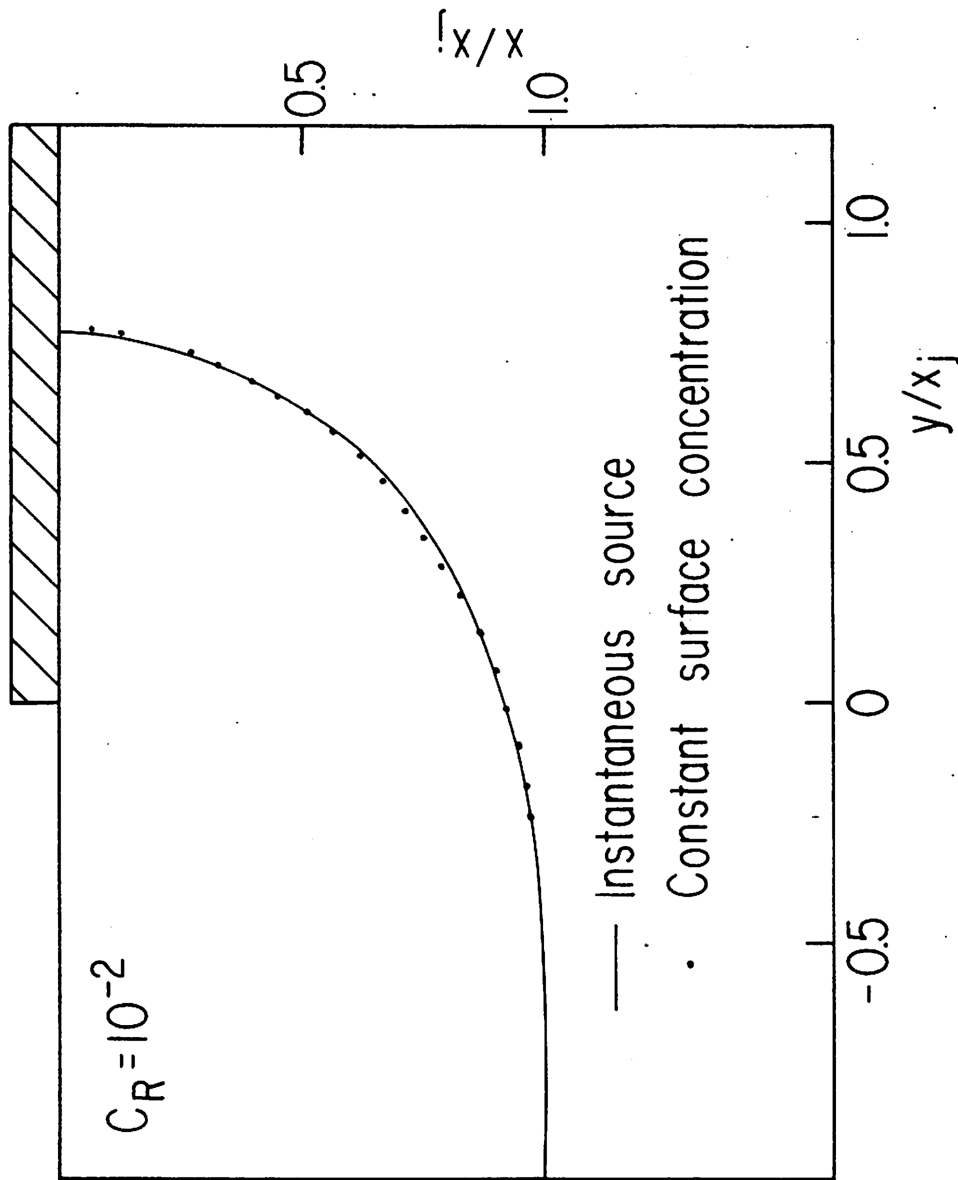

Fig. 3 c.

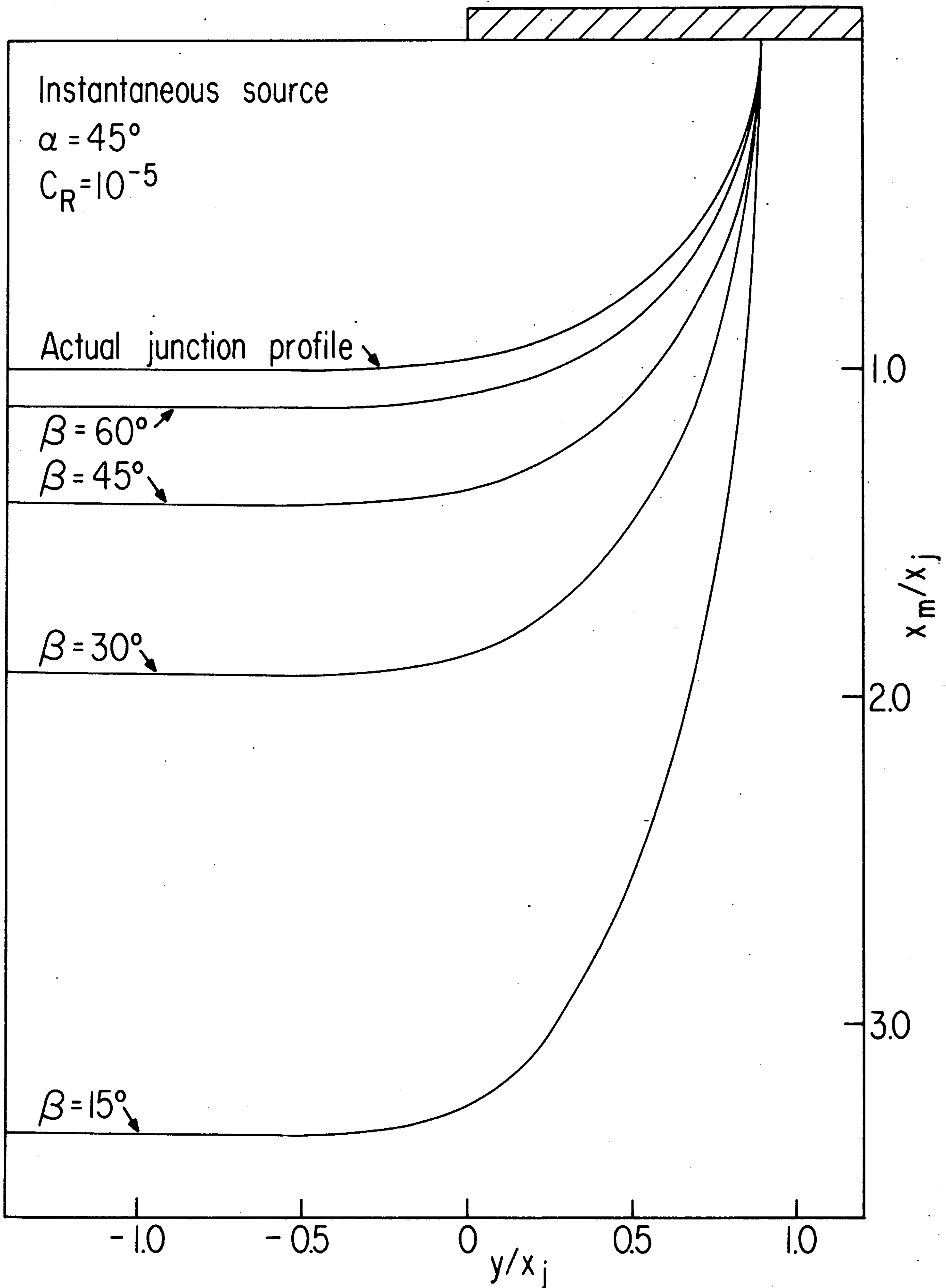

Fig. 4.

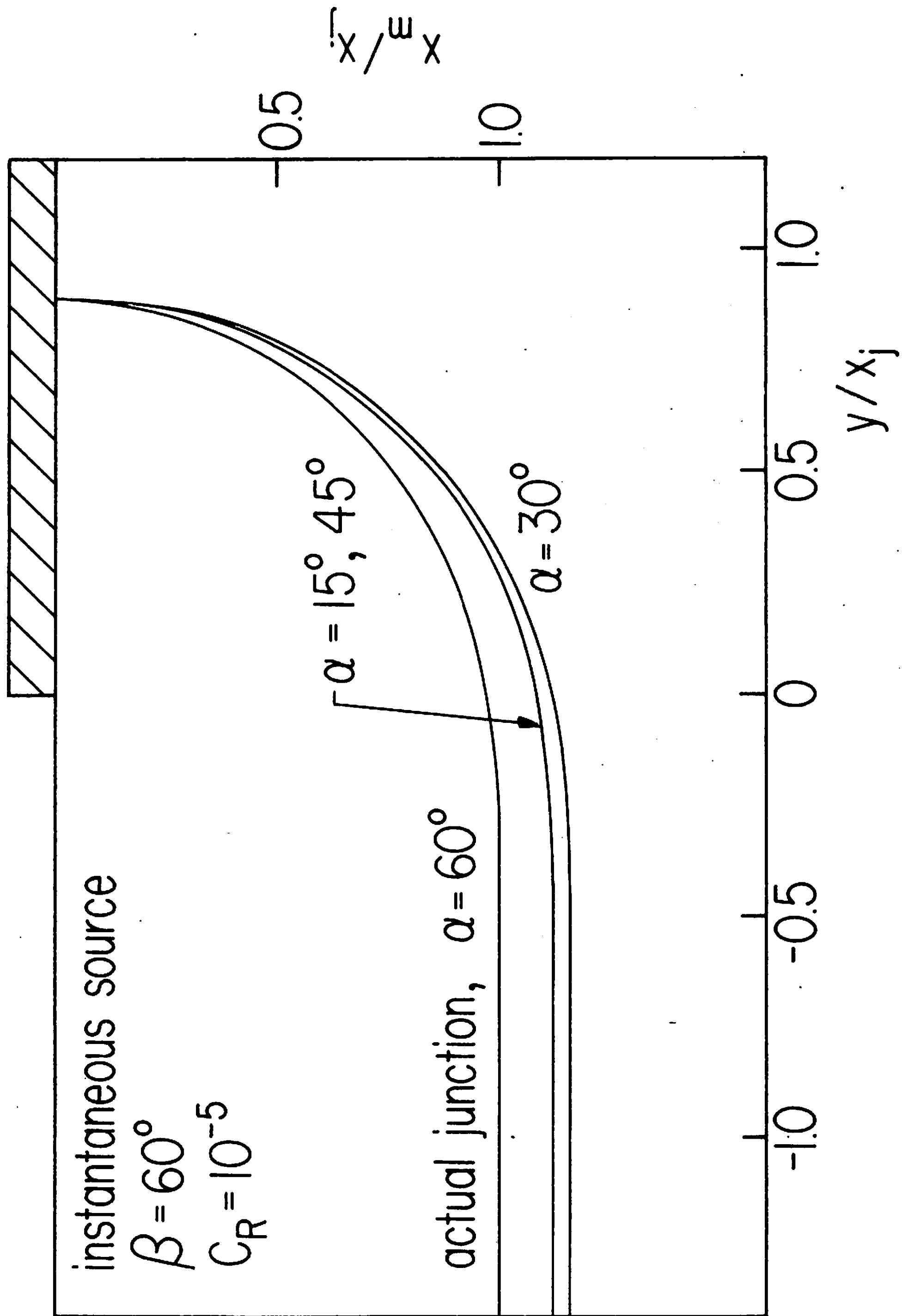

Fig. 5.

a)

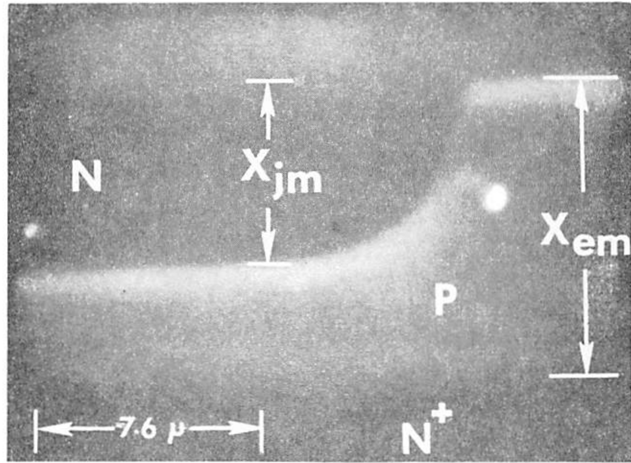

b)

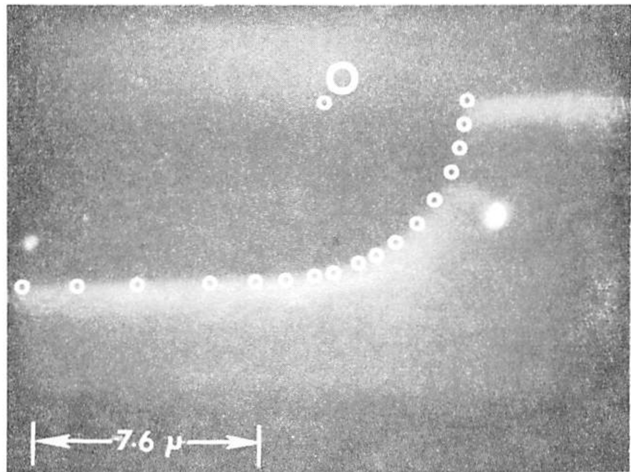

Fig. 6.

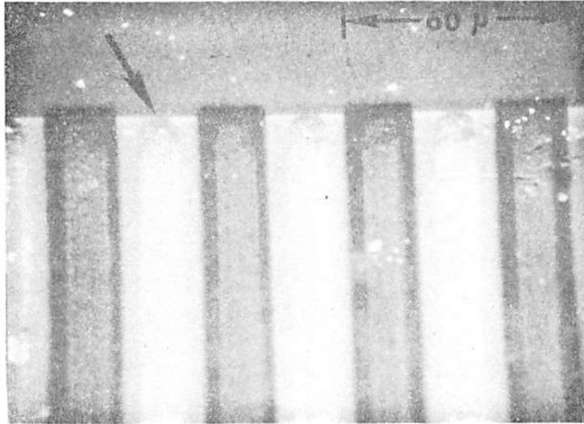

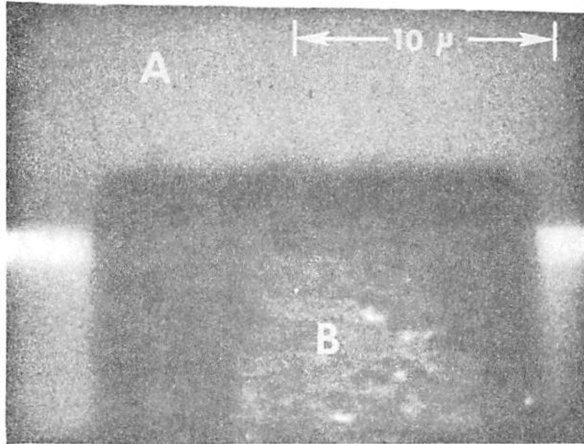

Fig. 7.

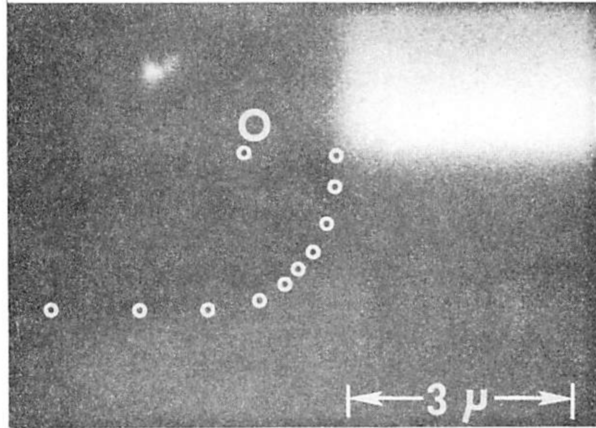

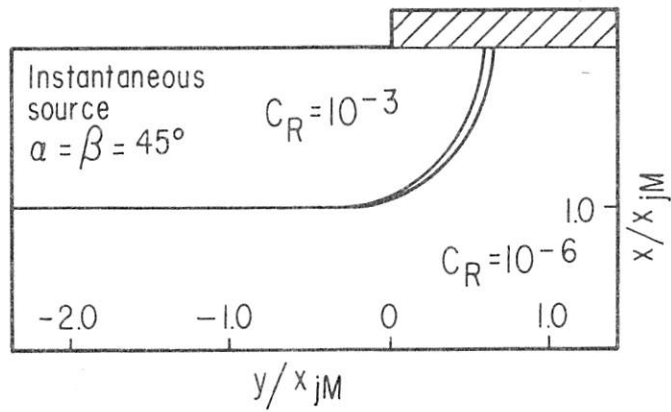

Fig. 8.

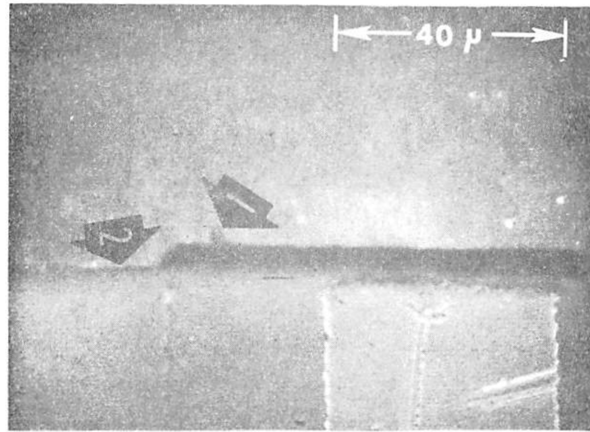

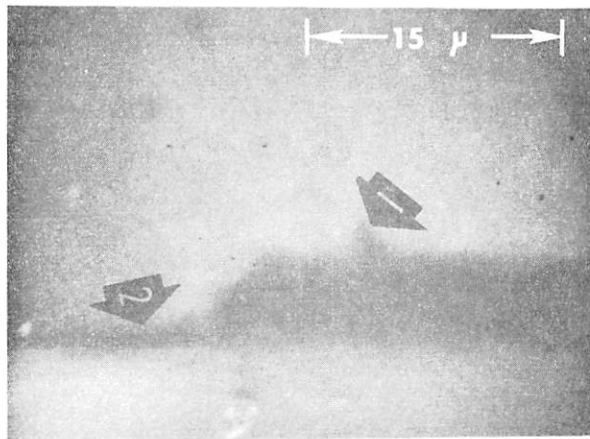

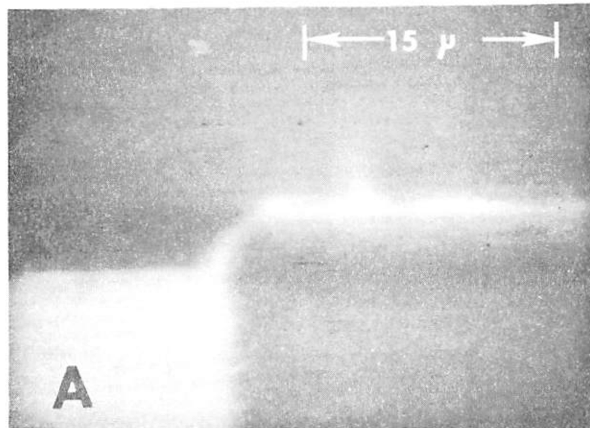

Fig. 9.

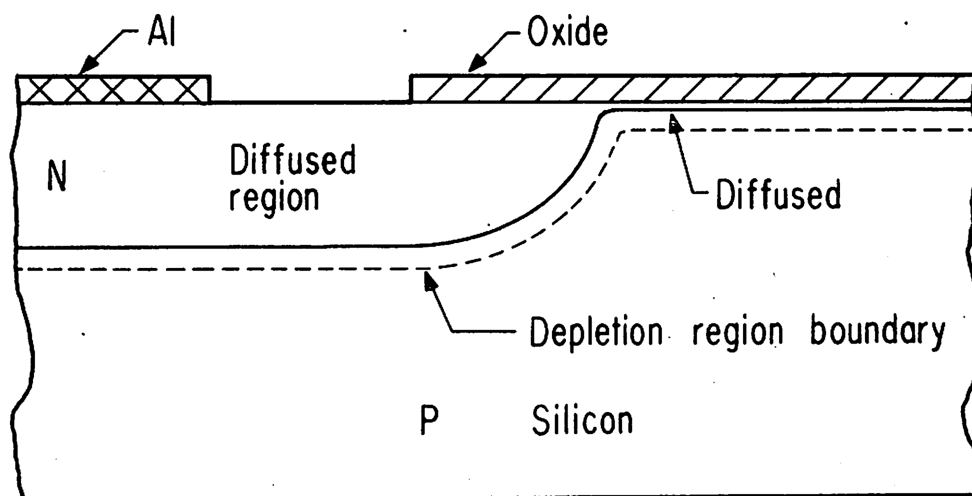

Fig. 10.

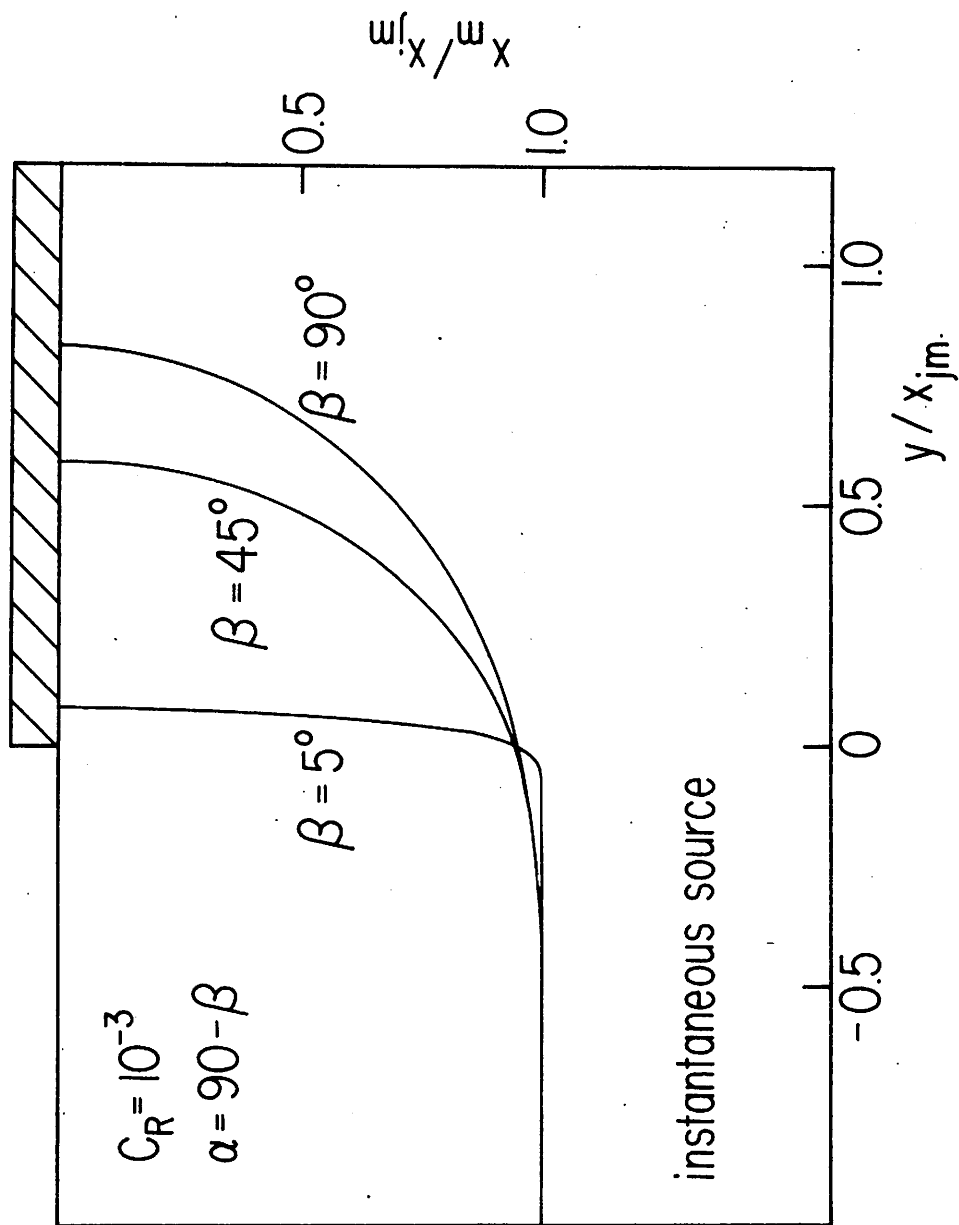

Fig. 11.